Materials Chemistry and Physics 145 (2014) 75–81

Contents lists available at ScienceDirect

Materials Chemistry and Physics

journal homepage: www.elsevier.com/locate/matchemphys

Size control in the formation of magnetite nanoparticles in the presence of citrate ions

Victor L. Kirillov [a,*], Dmitry A. Balaev [b], Sergey V. Semenov [b], Kirill A. Shaikhutdinov [b], Oleg N. Martyanov [a]

[a] Boreskov Institute of Catalysis, Siberian Branch of the Russian Academy of Sciences, 630090 Novosibirsk, Russia
[b] Kirensky Institute of Physics, Siberian Branch of the Russian Academy of Sciences, 660036 Krasnoyarsk, Russia

HIGHLIGHTS

- The citrate ion allows the size of the MNPs to be tuned in the range of 4–10 nm.
- Controlling the particle size around superparamagnetic threshold.
- Tuning the processes of agglomeration and the removal of the MNPs from solutions.
- The size control arises from the capping of the magnetite surface by citrate ions.

ARTICLE INFO

Article history:
Received 5 August 2013
Received in revised form
5 December 2013
Accepted 20 January 2014

Keywords:
Magnetic materials
Magnetic properties
Precipitation
Electron paramagnetic resonance

ABSTRACT

A one-pot synthesis method for the controllable growth of magnetite nanoparticles directly during the process of co-precipitation using citrate ions was developed. The effects of the concentration of citrate ions and the solution pH on the characteristics of magnetite particles with sizes in the range of 4–10 nm synthesized by the method of co-precipitation were studied. The results showed that the specified concentration of citrate ions allowed the preparation of magnetite particles with a definite size that exhibited superparamagnetic behaviour in a particular temperature range. As the concentration ratio of citrate to iron ions was increased from 0 to 0.11, the average size of the prepared magnetite particles decreased from 10.5 to 4.4 nm. As a result, the superparamagnetic blocking temperature decreased from 300 to 20 K, the saturation magnetisation decreased from 50 to 20 emu g^{-1}, and the average magnetic moment decreased from 8000 μ_B to 340 μ_B (at $T = 300$ K).

The obtained experimental data proved that the size effects of the magnetite nanoparticles can be attributed to the capping of the magnetite surface by adsorbed citrate ions. Thus, the suggested approach allows magnetite nanoparticles to be prepared with an optimum particle size around superparamagnetic threshold that prevents their irreversible agglomeration and simultaneously allows them to be removed from a solution at an acceptable rate.

1. Introduction

Submicron magnetic-particle-based materials find expanding applications, especially in the chemical and biomedical fields, such as in the magnetic separation of radioactive nuclides [1], the removal of heavy-metal cations [2,3] and arsenic [4], the magnetic separation and identification of pathogenic microorganisms [5], cancer hyperthermia [6], *in vivo* magnetic resonance visualisation [7], therapeutic drugs, gene and radionuclide delivery [8,9], and catalysis [10,11].

Currently, the development of catalysts and supports based on magnetic nanoparticles (MNPs) appears to be one of the most urgent problems regarding the application of magnetic transport systems for catalysis [12]. The need for the progress in this area is dictated by both environmental and economic issues and more so by new opportunities that arise from the use of magnetically separable catalysts. The reusability of expensive homogeneous catalysts supported on MNPs allows them to be considered as "quasi-homogeneous" systems that combine the advantages of homogeneous catalysts with the opportunity to remove them from the reaction mixture through simple magnetic separation procedures [13]. Considerable progress has been achieved in the application of magnetic particles and MNP-based catalysts for cross-coupling reactions [14,15], hydrogenation [16,17],

* Corresponding author. Tel.: +7 3833269689.
E-mail address: VKirillov@catalysis.ru (V.L. Kirillov).

0254-0584/$ – see front matter © 2014 Elsevier B.V. All rights reserved.
http://dx.doi.org/10.1016/j.matchemphys.2014.01.036

hydroformylation [18], oxidation and epoxidation [19,20], enantioselective [21,22], and acid–base processes [23], among others [24].

The required properties (e.g., the particle size, the chemical and thermal stability, the magnetic characteristics, the surface state, etc.) for MNPs and MNP-based catalysts vary depending on the application area. For example, micron- and submicron-sized magnetic particles with low toxicity and a high saturation magnetisation value are needed in biomedicine to provide targeted drug delivery and the complete removal of the MNPs by a magnetic field [25].

One of the critical factors for a catalyst system is a high specific surface area and the absence of diffusion difficulties. In this regard, MNPs used for magnetically separable catalysts should be small (~5–50 nm). In addition, the characteristics of magnetic carriers, which can vary due to surface functionalisation, should provide a sufficient rate for the complete removal of the catalysts and simultaneously prevent irreversible agglomeration of particles during the course of a catalytic reaction to maintain a high specific surface area. Catalytic systems based on MNPs should also be stable at high temperatures in reaction media with various acidity levels. Therefore, the development of methods for the synthesis of stable powders with a mean MNP size in the range of ~5–50 nm and a narrow size distribution of particles that exhibit similar magnetic characteristics is necessary.

Chelating ions are known to stabilise highly dispersed nanoparticles. Surface-adsorbed chelating agents form a polyanionic coating that provides both steric and electrostatic potential barriers and prevents the aggregation of nanoparticles due to intermolecular interactions and magnetic dipole–dipole interactions between MNPs. For example, phosphate ions ($H_2PO_4^-$) efficiently inhibit nucleation and aggregation of magnetite nanoparticles synthesized by oxidative co-precipitation of Fe^{2+} from an acidic solution under heating [26]. This approach allowed particles with sizes smaller than the superparamagnetic threshold for the given material to be prepared. The authors attributed the reduction in particle size not only to the inhibiting effect of phosphate ions, but also to the formation of Fe–phosphate complexes. The influence of chelating agents (e.g., citrate, oxalate, phosphate ions, EDTA) on the formation of haematite particles has also been reported elsewhere [27].

Polyanionic coatings, including the citrate-based ones, are widely used for post-synthesis nanoparticles and MNPs stabilisation [28–33].

However, little research devoted to the application of a capping agent during the MNPs synthesis has been reported. In one example [34], the authors obtained nanocrystalline cobalt-doped magnetite $Co_xFe_{3-x}O_4$ ($0.05 \leq x \leq 0.20$) using preliminarily synthesized citrate complexes. In another example [35], cobalt nanoparticles were synthesized via the reduction of $CoCl_2$ with sodium borohydride in the presence of citric acid. The authors found that, as the molar ratio between citrate and Co^{2+} ions was increased from 0.01 to 1, the size of the cobalt nanoparticles decreased by a factor of almost 5 (from 78 nm to 17 nm). Other authors [36] have suggested a method for the synthesis of haematite nanoparticles by the oxidation of magnetite, which, in turn, was prepared by co-precipitation in the presence of various concentrations of citrate ions. The size of haematite nanoparticles decreased from 8 to 2 nm as the ratio of citrate ions to iron ions was increased from 0 to 0.03. Unfortunately, the size and magnetic characteristics of the magnetite nanoparticles were not studied.

Despite the publication of numerous papers devoted to the preparation of magnetic particles, the problem of controlling the synthesis of iron-oxide particles to produce particles with a certain structure with sizes on the order of a few nanometres is still a challenge, especially with respect to the preparation of nanoparticles for catalytic applications. The currently available information indicates that the development of a one-pot method for the synthesis of magnetite nanoparticles directly through co-precipitation using citrate ions to control the growth is possible.

Here, we report the effects of citrate ions during co-precipitation on the size-dependent properties of magnetite particles. Structural and size characteristics of the particles were studied by XRD (X-ray diffraction) and HR TEM (high-resolution transmission electron microscopy) methods. As expected, the studies of the magnetostatic and the magnetic resonance properties of the synthesized systems showed the transition from superparamagnetic behaviour to a ferrimagnetic state with nonzero residual magnetisation in the given size range at room temperature. The citrate ions allowed the controlled synthesis of magnetite nanoparticles in the size range of 4–10 nm with a rather narrow particle size distribution. Thus, the suggested approach enables the average size of the magnetite nanoparticles to be tuned to within a few nanometres around superparamagnetic threshold; it also allows the magnetic properties to be tuned to those required for the magnetic transport systems in catalysis (a) to avoid irreversible aggregation and simultaneously allows (b) complete removal of the MNPs from the system (within an acceptable time period).

2. Materials and methods

2.1. Materials

The following reagents of chemical purity grade were used: citric acid monohydrate (Acros Organics), 99.5%; 23.5% ammonia aqueous solution (Sigma–Aldrich), ≥99.99%; $FeSO_4 \cdot 7H_2O$ (Acros Organics), 99+%; $FeCl_3 \cdot 6H_2O$ Sigma–Aldrich, (≥98%). To prepare the initial solution of Fe^{2+} and Fe^{3+} salts with a total iron concentration of 0.900 mol L^{-1}, $FeSO_4 \cdot 7H_2O$ and $FeCl_3 \cdot 6H_2O$ were dissolved in distilled (deoxygenated) water at a Fe^{3+}/Fe^{2+} molar ratio of 2.

The obtained solution was filtered through a filter paper (pore diameter 1–2.5 μm) and was used within two weeks after being prepared.

2.2. Synthesis of Fe_3O_4

Magnetite particles were synthesized by co-precipitating Fe^{2+} and Fe^{3+} salts ($[Fe^{3+}]/[Fe^{2+}] = 2$) in the presence of citrate ions. Total concentration of Fe^{2+} and Fe^{3+} ions was 0.15 mol L^{-1}. The molar ratio of citrate to iron ions varied from 0 to 1.2, and the pH varied from 7.5 to 11.6. We performed the synthesis under an Ar atmosphere at room temperature (18–24 °C) by mixing Fe^{2+} and Fe^{3+} solution under intensive mechanical stirring (500 rpm) with solution of ammonium hydroxide and citric acid in preliminarily deoxygenated water. Magnetite nanoparticles were aged for 3 days at room temperature before characterization.

2.3. Testing methods

pH measurements were performed using a Hanna pH 213 pH meter equipped with a regular refillable glass electrode.

High-resolution transmission electron microscopy (HR TEM) images were obtained with a JEOL JEM-2010 microscope with a resolution of 1.4 Å operated at an accelerating voltage of 200 kV. The size distribution of the nanoparticles was calculated based on a representative set of HR TEM images taken at different areas of the sample. The number of measured particles was 546, 557 and 491 for samples Cit-0, Cit-20 and Cit-100, respectively.

The X-ray diffraction (XRD) analysis was performed using an XTRA powder diffractometer (Switzerland) equipped with a CuK_α

radiation source (wavelength, $\lambda = 1.5418$ Å) and operated at a scanning step of 0.050° 2θ and an accumulation time of 3 s. The mean size of the coherent scattering region of crystallites was calculated from the half-width of the XRD peak ($2\theta = 35.57°$) by the Scherrer equation: $d = K\cdot\lambda/(\beta\cdot\cos\cdot(\theta))$, where d is the mean size of the coherent scattering region of crystallites; K is a dimensionless shape factor (0.9); λ is the X-ray wavelength; β is the line broadening at half the maximum intensity of the XRD peak, after subtracting the instrumental line broadening, in radians; θ is the Bragg angle.

The magnetisation of the samples was measured using a PPMS-6000 vibrational magnetometer within the temperature range of 4.2–300 K. Magnetite nanoparticles were placed in a paraffin matrix for magnetic measurements via a supersonic treatment (44 kHz, 1–10 min) of a hot mixture of oleic acid, a magnetite water suspension and paraffin. The concentration of magnetite in the paraffin was 0.46, 0.25 and 0.15 (wt.%) for samples Cit-0, Cit-20 and Cit-100, respectively, to minimise the interparticle magnetic dipole–dipole interactions. The diamagnetic background was subtracted from the experimental magnetic measurement data.

Electron-spin resonance (ESR) spectra were obtained using a Bruker ELEXSYS-500 radiospectrometer at the X-band frequency ($\nu = 9.4$ GHz). The spectra were recorded at room temperature using a 100 kHz modulation frequency.

3. Results and discussion

Using the described synthesis procedure, we prepared a series of samples with different molar ratios of citrate to iron ions and different pH values. Table 1 presents the characteristics of three samples synthesized at pH 9.5: Cit-0, Cit-20 and Cit-100. The positions and intensities of the peaks in the XRD patterns indicate that the Cit-0 and Cit-20 samples consist of iron oxide magnetite nanoparticles (Fig. 1), in accordance with the previously reported literature data (International Centre for Diffraction Data (ICDD) card 88-0315). Broadening of the XRD peaks in the pattern of Cit-100 was observed, which indicated that the average crystallite size of the magnetite particles was smaller than those in samples Cit-0 and Cit-20. Table 1 presents the mean sizes of the coherent scattering regions for Fe_3O_4 particles in the samples, as calculated from the half-width analyses of the XRD peaks.

According to the HR TEM data, the average sizes of the Fe_3O_4 particles are 4.4, 8.3 and 10.5 nm for samples Cit-100, Cit-20 and Cit-0, respectively (Fig. 2). According to the regular statistical two-sample t-test (Cit-20 and Cit-0) shows the difference in average sizes of the particles greater than 1.77 nm at the 0.05 level of significance.

As the citrate concentration was increased, the average size of the magnetite particles decreased, and the particle size distribution became narrower. Indeed, in the absence of citrate ions (Cit-0), the ratio of standard deviation to the mean size was 0.4, whereas this value was 0.23 for the Cit-100 sample. A combined analysis of the XRD and HR TEM data shows a good agreement between the average particle size and the mean size of the coherent scattering region only for the Cit-0 sample. This result implies that Fe_3O_4 particles in sample Cit-0 are magnetite crystals, whereas samples Cit-20 and Cit-100 consist of polycrystalline Fe_3O_4 particles, likely with an X-ray-amorphous surface layer.

Table 1
The ratio between citrate and iron ions in solutions and the corresponding size characteristics of the magnetite particles according to XRD and HR TEM data.

	Cit-0	Cit-20	Cit-100
$\nu_{citrate}/\nu_{Fe}$	0	0.0184	0.1105
Mean size of coherent scattering region, nm (XRD data)	10.3	3.6	1.4
Mean size, nm (HR TEM data)	10.5	8.3	4.4
Standard deviation, nm (HR TEM data)	4.2	2.9	1.0

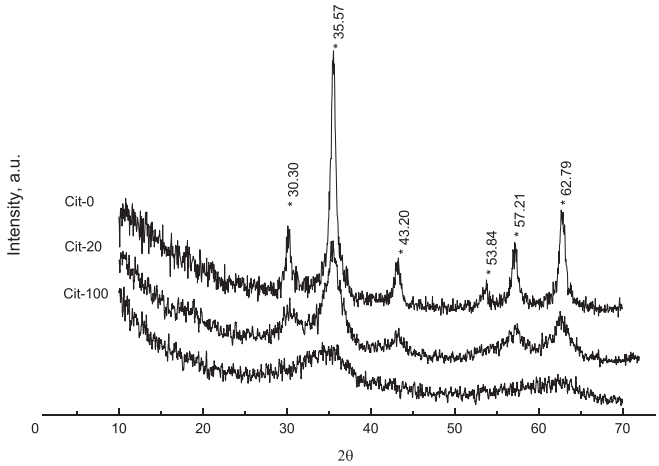

Fig. 1. XRD patterns for the Cit-0, Cit-20 and Cit-100 samples.

The particle size appears to depend solely on the relative concentration of citrate ions at the given pH and appears to be independent of the initial concentration of iron ions. Fig. 3 shows the ESR line peak-to-peak widths of magnetite particles synthesized at pH 9.5 as a function of the relative concentration of citrate ions ($\nu_{citrate}/\nu_{Fe}$) for solutions with total iron concentrations of 0.15 mol L^{-1} and 0.05 mol L^{-1}. The width and shape of ESR adsorption lines are known to be sensitive to slight variations in the size, shape and structure of MNPs. For this reason, a comparative analysis of ESR and HR TEM data for the given species allows a qualitative conclusion concerning the size characteristics of the magnetite particles to be drawn. A tripling of the initial iron concentration (from 0.05 to 0.15 mol L^{-1}) at the given pH does not affect the ESR linewidth, which proves that the influence of this parameter on the final particle size is insignificant.

As the relative concentration of citrate ions was increased, the ESR line became narrower and shifted toward a stronger magnetic field region (to $g = 2.00$). The ESR spectrum of the Cit-100 sample ($\nu_{citrate}/\nu_{Fe} = 0.11$) exhibits the narrowest line (Fig. 3 (inset)), and its shape is typical of that of superparamagnetic particles [37]. The absence of a broad component in the ESR spectrum of Cit-100 indicates a narrow particle size distribution and the absence of a noticeable amount of large particles, which also corroborates the microscopy data. In turn, the absence of a narrow line in the ESR spectrum of the sample prepared without citrate ions indicates the absence of a noticeable amount of superparamagnetic particles with a size less than 4 nm in the Cit-0 sample (Fig. 3 (inset)).

The citrate ion, as a "hard" ligand, is known to form more stable complexes with Fe^{3+} ions than with Fe^{2+} ions [38], which should lead to an increase in the threshold pH at which the precipitation of Fe^{3+} occurs; i.e., the pH values at which precipitation of Fe^{2+} and Fe^{3+} ions begins (7.5 and 2.3, respectively [39]) converge in the presence of citrate ions, which facilitates the formation of polynuclear iron oxide precursors of magnetite particles with stoichiometric Fe^{3+}/Fe^{2+} ratios. This stoichiometric Fe^{3+}/Fe^{2+} ratio leads to an increase in the speed at which the particles form and to a reduction in their size.

In the course of nucleation and growth, citrate anions adsorb onto the surface of magnetite particles. Simultaneously, the total surface area of Fe_3O_4 particles decreases as the characteristic particle size increases. Consequently, the concentration of citrate ions

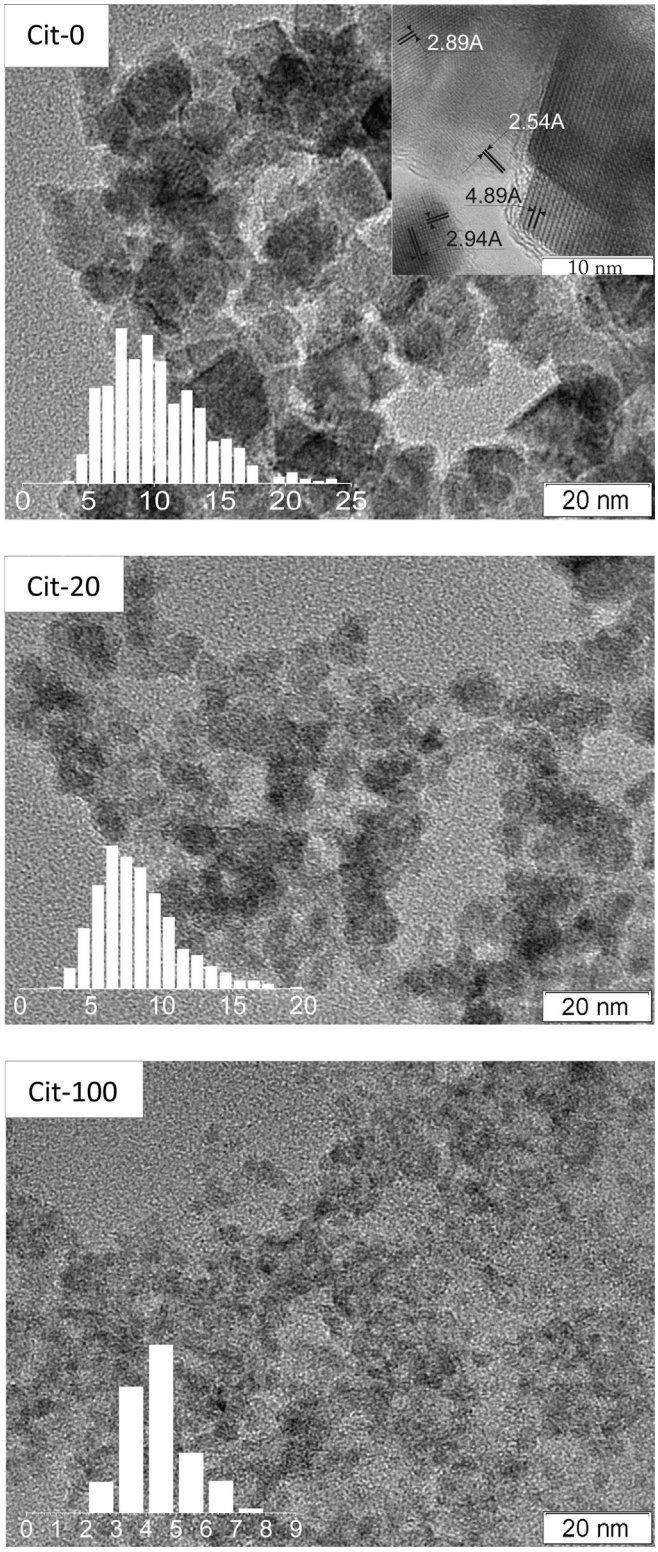

Fig. 2. HR TEM data and the particle size distribution for the Cit-0, Cit-20 and Cit-100 samples. The d-spacings are shown for the Cit-0 sample: 4.85, 2.97, 2.54 Å, which correspond to the {111}, {220} and {311} crystallographic planes of the magnetite structure.

in the solution becomes sufficient to create a surface layer of adsorbed anions, which inhibits further particle growth, as a certain particle size is reached. Indeed, the average size of Fe_3O_4 particles decreases in proportion to the $\nu_{citrate}/\nu_{Fe}$ ratio at which the

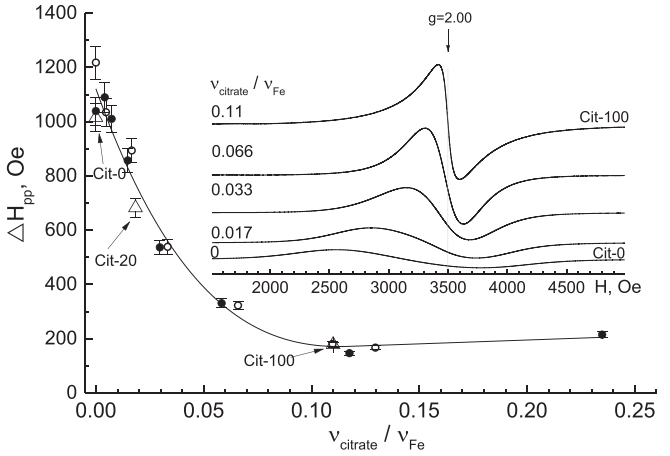

Fig. 3. ESR line peak-to-peak width at 300 K (ΔH_{pp}) for magnetite particles synthesised at pH 9.5 as a function of the relative concentration of citrate ions ($\nu_{citrate}/\nu_{Fe}$). The results are shown for solutions with total iron concentrations of 0.15 mol L^{-1} – (○) and 0.05 mol L^{-1} – (●). The values of ΔH_{pp} for the Cit-0, Cit-20 and Cit-100 samples are marked by (△) symbols. The narrowing of the ESR spectra as the $\nu_{citrate}/\nu_{Fe}$ was increased is demonstrated, including ESR spectra for Cit-0 and Cit-100 samples.

particles were synthesized. Of course, in the case where size effects arise from the high relative content of surface atoms and where the variation in the chemical potential of the nanoparticles is considerable, the indicated regularities could be violated.

A lower solution pH resulted in a stronger effect of citrate ions on the particle size. According to the ESR data, as the pH was decreased from 11.6 to 10.3, an equally narrow ESR line was obtained using one-fourth the respective citrate concentration (Fig. 4). The observed effect can be explained by a decrease in the density of negative charges on the surface of magnetite nanoparticles at low pH values. Indeed, the density of the surface negative charge of magnetite nanoparticles is known [40] to increase considerably at pH levels greater than 9, which impedes adsorption of negatively charged citrate anions. Thus, a higher solution pH results in a greater concentration of citrate ions required for the formation of a polyanionic coating that inhibits particle growth.

Fig. 5 shows the temperature dependences of the magnetic moments $M(T)$ for the samples under investigation. The dependences were obtained in the ZFC (zero-field cooled) and FC

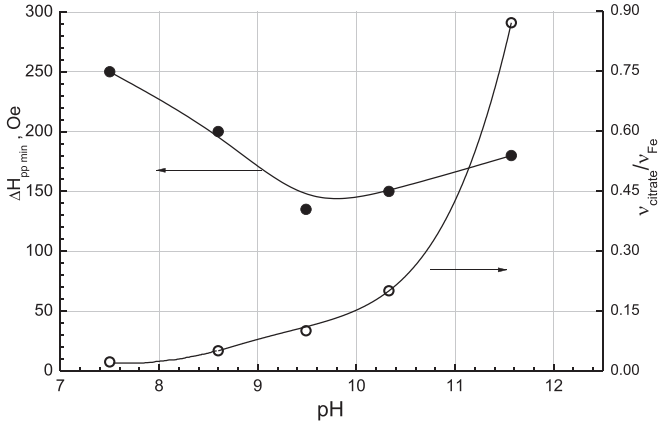

Fig. 4. The change in the minimal peak-to-peak width of ESR spectra ($\Delta H_{pp\ min}$) that can be achieved by the variation of the relative citrate ion concentration ($\nu_{citrate}/\nu_{Fe}$) as a function of the solution pH. The appropriate values of $\nu_{citrate}/\nu_{Fe}$ (that allow the minimum ESR linewidth to be achieved) are shown on the right side of the figure.

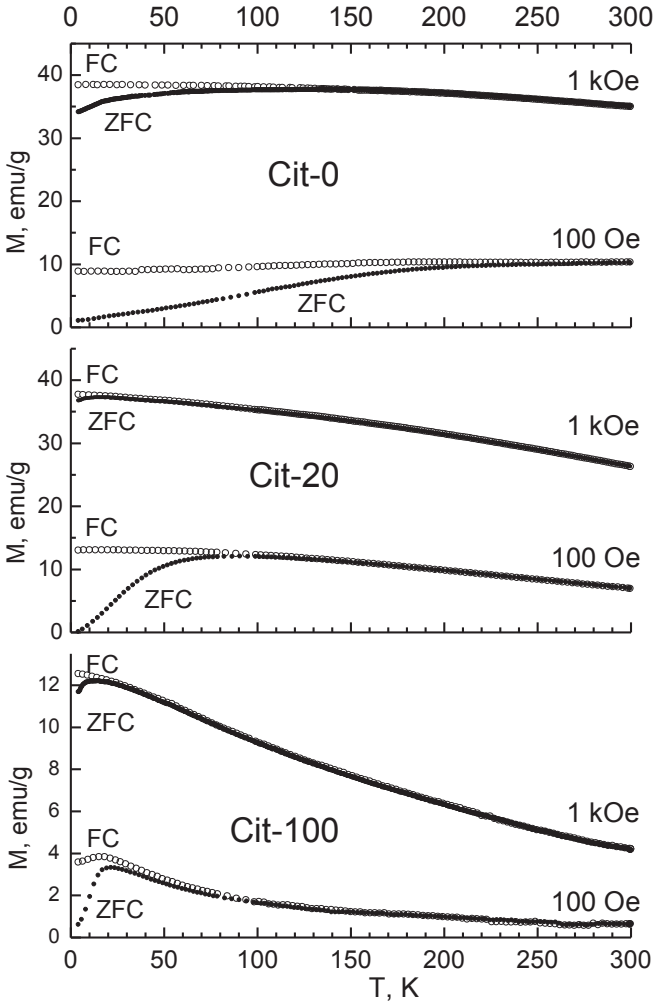

Fig. 5. Temperature dependences of the magnetic moments of the samples in FC and ZFC regimes in external magnetic fields of $H = 100$ Oe and 1 kOe.

(field cooled) regimes in magnetic fields of 100 Oe and 1 kOe. The dependences $M(T)_{ZFC}$ of the Cit-20 and Cit-100 samples obtained in the $H = 100$ Oe field exhibit maxima at temperatures of 90 and 20 K, respectively (Fig. 5). A divergence between the $M(T)_{FC}$ and $M(T)_{ZFC}$ dependences was observed at higher temperatures (~200 K for Cit-20 and ~100 K for Cit-100). As the external field was increased, the maximum of the $M(T)_{ZFC}$ dependence and the temperature of the irreversible magnetisation behaviour shifted toward the low-temperature region. For the Cit-0 sample, the discrepancy between the $M(T)_{FC}$ and $M(T)_{ZFC}$ dependences was observed at a higher temperature (~300 K) compared to those of samples Cit-20 and Cit-100. In the external $H = 1$ kOe field, the $M(T)_{ZFC}$ dependence for sample Cit-0 also exhibited a broad maximum near 150 K. This behaviour is unambiguously related to the superparamagnetic state of the magnetite particles in the samples and to the existence of a blocking temperature T_B. The T_B values determined in a weak magnetic field were ≈90 and 20 K for the Cit-20 and Cit-100 samples, respectively, whereas the blocking temperature for the Cit-0 sample was ~300 K (Fig. 5). Notably, no anomalies were observed in the $M(T)$ dependences near the Verwey temperature (120 K), which is typical for bulk magnetite and Fe_3O_4 particles with a size of approximately 50 nm [41–43].

Fig. 6 presents the magnetic field dependences of the magnetic moment $M(H)$ at $T = 4$ K for the samples Cit-0, Cit-20, and Cit-100.

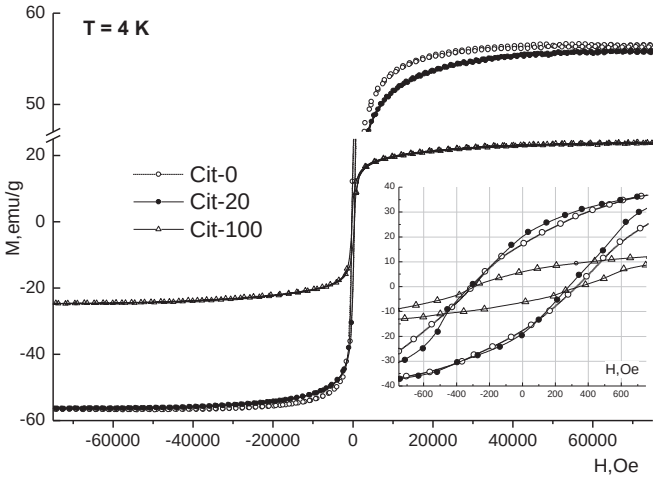

Fig. 6. $M(H)$ dependences for Cit-0, Cit-20 and Cit-100 samples at $T = 4$ K. Insert: the range of weak magnetic fields.

For superparamagnetic particles at $T < T_B$, the dependences $M(H)$ are well known to be determined by the competition of the Zeeman energy $\mu_P \cdot H$ (where μ_P is the magnetic moment of a particle), the effective magnetic anisotropy energy, and thermal fluctuations. At $T = 4$ K ($T < T_B$), the samples are saturated in sufficiently strong magnetic fields: ~45 kOe and ~60 kOe for the Cit-0 and Cit-20 samples, respectively. In this case, the saturation magnetisation M_S values were 56.5 emu g^{-1} for sample Cit-0 and 55.9 emu g^{-1} for sample Cit-20. For the Cit-100 sample, which contained the smallest particles, the approximate M_S value for this sample was approximately 25 emu g^{-1}.

The observed M_S values are smaller than the saturation magnetisation values of bulk magnetite ($M_{S\ bulk} \approx 92$ emu g^{-1}) [44]. Such behaviour of the saturation magnetisation is known and is typical for Fe_3O_4 nanoparticles [43–46]. A decrease in M_S is usually attributed to the surface layer of Fe_3O_4 particles, where the magnetic moments of iron atoms are disordered and do not contribute to the resulting magnetic moment of a particle. For example, for cubic particles, this model in the first approximation yields the expression [44]:

$$M_S = M_{S\ bulk} \cdot (1 - 2a/d)^3, \quad (1)$$

where a is the thickness of the "magnetically dead" surface layer, and d is the particle size. For the investigated samples, the values of a obtained using equation (1), the average particle size $<d>_{HR\ TEM}$ and M_S at 4 K are given in Table 2. As evident from the results in the table, the thickness of the "magnetically dead" layer is approximately 0.7 nm, which allows the average size of the magnetically ordered core of the particles to be estimated according to $d^* = <d>_{HR\ TEM} - 2a$ (Table 2).

The experimentally observed saturation magnetisation (M_S) is mainly determined by the magnetically ordered core size ($d^* = <d>_{HR\ TEM} - 2a$) as well as the size distribution of the particles. Therefore the sufficiently smaller value of d^* and the absence of the relatively large particles in the Cit-100 sample result to considerably smaller M_S for this sample in comparison with Cit-0 and Cit-20 samples.

The coercivity value H_c for samples Cit-0, Cit-20, and Cit-100 at $T = 4$ K was approximately the same: ~300 Oe (see the inset in Fig. 6). This value is typical for magnetite superparamagnetic particles at temperatures less than T_B and is in a good agreement with the available data [43,46]. As the temperature was increased, the

Table 2
Sample characteristics deduced from measurements of their magnetic properties.

Sample	Average particle size $<d>_{HR\ TEM}$, nm	M_S (4 K) emu g^{-1}	Magnetically disordered layer thickness a, nm	Magnetically ordered core size d^*, nm ($<d>_{HR\ TEM} - 2a$)	Particle moment $<\mu_P>$, μ_B	$(<\mu_P>/<\mu_P>_{Cit\text{-}100})^{1/3}$	$d^*/d^*_{Cit\text{-}100}$
Cit-0	10.5	56.5	0.79	8.9	8000	2.8	3.2
Cit-20	8.3	55.9	0.64	7.0	2500	1.9	2.5
Cit-100	4.4	25	0.77	2.8	340	1	1

coercivity decreased. At $T = 300$ K, a hysteresis-free behaviour of $M(H)$ and an absence of residual magnetisation were observed for the Cit-20 and Cit-100 samples (Fig. 7). For the Cit-0 sample at $T = 300$ K (i.e., at $T \sim T_B$), a small hysteresis of $M(H)$ was detected in an $H = 100$ Oe magnetic field, and this hysteresis vanished at $H > 5$ kOe; the coercivity was $H_c \sim 30$ Oe, and the residual magnetisation was $M_S \sim 4$ emu g^{-1}.

The magnetisation curve for an ensemble of noninteracting identical superparamagnetic particles is described by the Langevin function $L(x) = \coth(x) - 1/x$, where $x = \mu_P H/kT$ (k is the Boltzmann constant). For a real system, the use of a distribution function for the magnetic moments that is similar to the particle size distribution observed in the experiment is necessary. Indeed, the magnetic moment of a superparamagnetic particle with ferrimagnetic ordering in the first approximation is proportional to the number of atoms that compose this particle and, consequently, is proportional to the particle volume. Therefore, the size distribution function $f(d)$ according to the HR TEM data and the magnetic moment distribution function $f(\mu_P^{1/3})$ should be consistent with one another for different samples. The log-normal magnetic moment distribution $f(\mu_P) = (\mu_P \cdot s \cdot (2\pi)^{1/2})^{-1} \exp\{-[\ln(\mu_P/n)]^2/2s^2\}$, where s is the dispersion and where the average magnetic moment of particles is $<\mu_P> = n \cdot \exp(s^2/2)$, can be used. Then, the magnetisation curve that describes the behaviour of superparamagnetic particles at $T > T_B$ is given by the expression

$$M(H) = N_P \int_{\mu_{min}}^{\mu_{max}} L(x) f(\mu_P) \mu_P d\mu_P, \quad (2)$$

where the variable parameters are the distribution function setting ($<\mu_P>$, s) and the number of particles (N_P) that determine the total magnetic moment M_S.

Fig. 7 shows the results of the best fit of the experimental dependence of $M(H)$ at $T = 300$ K using equation (2). The best agreement with experimental data is obtained at $<\mu_P> = 8000\ \mu_B$, $s = 1.4$, and $M_S = 53.19$ emu g^{-1} for the Cit-0 sample; at $<\mu_P> = 2500\ \mu_B$, $s = 1.55$, and $M_S = 48.9$ emu g^{-1} for the Cit-20 sample; and at $<\mu_P> = 340\ \mu_B$, $s = 1.65$, and $M_S = 20.27$ emu g^{-1} for the Cit-100 sample. The M_S values calculated by equation (2) in the limit of strong magnetic fields gives the saturation magnetisation of the particles at $T = 300$ K. The distribution function $f(\mu_P^{1/3})$ reproduced sufficiently well the shape of the particles size distribution determined by HR TEM.

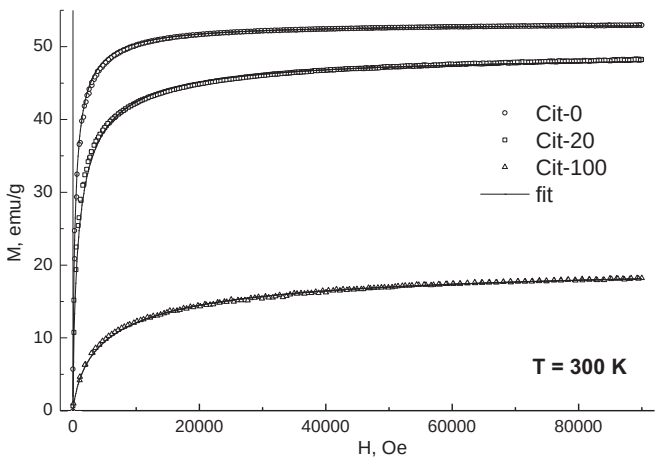

Fig. 7. The $M(H)$ dependences for Cit-0, Cit-20 and Cit-100 samples at $T = 300$ K (symbols). Solid lines are the results of the best fit using equation (2).

Table 2 presents the values of $(<\mu_P>/<\mu_P>_{Cit\text{-}100})^{1/3}$ and the relative sizes of the effective magnetic cores for the different particles, $d^*/d^*_{Cit\text{-}100}$. These values are in satisfactory agreement, which indicates that the magnetic data analysis is adequate. Despite the significant difference between their coherent scattering regions (according to the XRD data) and their average magnetic moments $<\mu_P>$, the Cit-0 and Cit-20 samples exhibit approximately the same saturation magnetisations. The obtained magnetite nanoparticles are stable in ethanol, paraffin, and a water–ammonia solution of ammonium chloride (pH ~ 9.5) for prolonged periods. The long-term storage of the samples does not change the sizes and magnetic characteristics of the MNPs.

4. Conclusions

A one-pot synthesis using citrate ions as an additive for the controllable growth of magnetite nanoparticles directly via a co-precipitation process was developed. The proposed method enables the size-controlled synthesis of magnetite particles in the range of 4–10 nm with the use of citrate ions. As expected, the obtained particles exhibited superparamagnetic behaviour over a wide temperature range, as proved by magnetic resonance and magnetostatic measurements. An increase in the relative citrate concentration from 0 to 0.11 resulted in a decrease in the average size of the obtained magnetite particles from 10.5 to 4.4 nm. As a result, the superparamagnetic blocking temperature decreased from 300 to 20 K, the saturation magnetisation decreased from 50 to 20 emu g^{-1}, and the average magnetic moment decreased from 8000 μ_B to 340 μ_B (at $T = 300$ K). The observed size effects in the formation of magnetite nanoparticles were attributed to the capping of the magnetite surface by adsorbed citrate ions.

The suggested approach allows the synthesis of the magnetite particles to be tuned to provide the required size and magnetic characteristics to enable the transition from ferrimagnetic to superparamagnetic behaviour in the specified temperature interval. This approach offers wide opportunities for the creation of magnetic transport systems for catalysis based on magnetic nanoparticles that provide an appropriate rate of complete removal of the catalysts from the solution and no irreversible agglomeration of the magnetic particles during the chemical reaction.

Acknowledgements

This work was supported by the Interdisciplinary Integration Project no. 45 of the Siberian Branch of the Russian Academy of Sciences for 2012–2014.

References

[1] R.D. Ambashta, S.M. Yusuf, M.D. Mukadam, S. Singh, P.K. Wattal, D. Bahadur, J. Magn. Magn. Mater. 293 (2005) 8–14.
[2] A.R. Mahdavian, M.A.-S. Mirrahimi, Chem. Eng. J. 159 (2010) 264–271.
[3] P.I. Girginova, A.L. Daniel-da-Silva, C.B. Lopes, P. Figueira, M. Otero, V.S. Amaral, E. Pereira, T. Trindade, J. Colloid Interface Sci. 345 (2010) 234–240.
[4] S. Luther, N. Borgfeld, J. Kim, J.G. Parsons, Microchem. J. 101 (2012) 30–36.
[5] H. Gu, P.-L. Ho, K.W.T. Tsang, L. Wang, B. Xu, J. Am. Chem. Soc. 125 (2003) 15702–15703.
[6] P. Moroz, S.K. Jones, B.N. Gray, J. Surg. Oncol. 77 (2001) 259–269.
[7] D.K. Kima, Y. Zhanga, W. Voitb, K.V. Raob, J. Kehrc, B. Bjelked, M. Muhammeda, Scr. Mater. 44 (2001) 1713–1717.
[8] Q.A. Pankhurst, J. Connolly, S.K. Jones, J. Dobson, J. Phys. D Appl. Phys. 36 (2003) 167–181.
[9] M. Răcuciu, D.E. Creangă, A. Airinei, Eur. Phys. J. E Soft Matter Biol. Phys. 21 (2006) 117–121.
[10] L. Qu, S. Tie, Microporous Mesoporous Mater. 117 (2009) 402–405.
[11] G.A. Bukhtiyarova, M.A. Shuvaeva, O.A. Bayukov, S.S. Yakushkin, O.N. Martyanov, J. Nanopart. Res. 13 (2011) 5527–5534.
[12] S. Shylesh, V. Schonemann, W.R. Thiel, Angew. Chem. Int. Ed. 49 (2010) 3428–3459.
[13] M.V. Barmatova, I.D. Ivanchikova, O.A. Kholdeeva, A.N. Shmakov, V.I. Zaikovskii, M.S. Mel'gunov, J. Mater. Chem. 19 (2009) 7332–7339.
[14] M.J. Jacinto, P.K. Kiyohara, S.H. Masunaga, R.F. Jardim, L.M. Rossi, Appl. Catal. A 338 (2008) 52–57.
[15] B. Baruwati, D. Guin, S.V. Manorama, Org. Lett. 9 (2007) 5377–5380.
[16] D.K. Yi, S.S. Lee, J.Y. Ying, Chem. Mater. 18 (2006) 2459–2461.
[17] Y. Jiang, Q. Gao, J. Am. Chem. Soc. 128 (2006) 716–717.
[18] T.-J. Yoon, W. Lee, Y.-S. Oh, J.-K. Lee, New J. Chem. 27 (2003) 227–229.
[19] L. Aschwanden, B. Panella, P. Rossbach, B. Keller, A. Baiker, ChemCatChem 1 (2009) 111–115.
[20] K. Schröder, B. Join, A.J. Amali, K. Junge, X. Ribas, M. Costas, M. Beller, Angew. Chem. Int. Ed. 50 (2011) 1425–1429.
[21] A. Schatz, M. Hager, O. Reiser, Adv. Funct. Mater. 19 (2009) 2109–2115.
[22] B. Panella, A. Vargas, A. Baiker, J. Catal. 261 (2009) 88–93.
[23] C. O'Dalaigh, S.A. Corr, Y. Gun'ko, S.J. Connon, Angew. Chem. 119 (2007) 4407–4410.
[24] M.A. Shuvaeva, I.V. Delii, O.N. Martyanov, O.A. Bayukov, E.I. Osetrov, A.A. Saraev, V.V. Kaichev, N.S. Sakaeva, G.A. Bukhtiyarova, Kinet. Catal. 52 (2011) 896–906.
[25] A.-H. Lu, E.L. Salabas, Ferdi Scheuth, Angew. Chem. Int. Ed. 46 (2007) 1222–1244.
[26] P.S. Sidhu, R.J. Gilkes, A.M. Posner, J. Inorg. Nucl. Chem. 40 (1978) 429–435.
[27] M. Ozaki, S. Kratohvil, E. Matijevic, J. Colloid Interface Sci. 152 (1992) 284–288.
[28] Y. Sahoo, H. Pizen, T. Fried, D. Golodnitsky, L. Burstein, C.N. Sukenik, G. Markovich, Langmuir 17 (2001) 7907–7911.
[29] T. Thi, H. Pham, C. Cao, S.J. Sim, J. Magn. Magn. Mater. 320 (2008) 2049–2055.
[30] P.C. Morais, R.L. Santos, A.C.M. Pimenta, R.B. Azevedo, E.C.D. Lima, Thin Solid Films 515 (2006) 266–270.
[31] A. Hajdua, E. Illes, E. Tombacz, I. Borbath, Colloids Surf. A 347 (2009) 104–108.
[32] N.V. Jadhav, A.I. Prasad, A. Kumar, R. Mishra, S. Dhara, K.R. Babu, C.L. Prajapat, N.L. Misra, R.S. Ningthoujam, B.N. Pandey, R.K. Vatsa, Colloids Surf. B 108 (2013) 158–168.
[33] Runa Ghosh, Lina Pradhan, Yensenbam Priyabala Devi, S.S. Meena, R. Tewari, Amit Kumar, Sachil Sharma, N.S. Gajbhiye, R.K. Vatsa, Badri N. Pandey, R.S. Ningthoujam, J. Mater. Chem. 21 (2011) 13388–13398.
[34] M.A. Ahmeda, N. Okashab, S.I. El-Deka, Ceram. Int. 36 (2010) 1529–1533.
[35] Y. Kobayashi, M. Horie, M. Konno, B. Rodrı.guez-Gonza, L.M. Liz-Marza, J. Phys. Chem. B 107 (2003) 7420–7425.
[36] A. Bee, R. Massart, S. Neveu, J. Magn. Magn. Mater. 149 (1995) 6–9.
[37] F. Gazeau, V. Shilov, J.C. Bacri, E. Dubois, F. Gendron, R. Perzynski, Yu.L. Raikher, V.I. Stepanov, J. Magn. Magn. Mater. 202 (535) (1999).
[38] G. Wilkinson (Ed.), Comprehensive Coordination Chemistry, vol. 4, Pergamon Press, 1987, p. 218.
[39] Yu.Yu. Lurie, Reference Book on Analytical Chemistry, sixth ed., 1989, p. 297. Chemistry-Moscow.
[40] I.V. Skvortsova, I.G. Gorichev, I.V. Sokolov, V.A. Ketchco, M.A. Fedchenko, Condens. Media Free Boundaries 9 (2007) 161–169.
[41] D. Sarkar, M. Mandal, K. Mandal, J. Appl. Phys. 112 (2012) 064318.
[42] R. Prozorov, T. Prozorov, S.K. Mallapragada, B. Narasimhan, T.J. Williams, D.A. Bazylinski, Phys. Rev. B 76 (2007) 054406.
[43] G.F. Goya, T.S. Berquó, F.C. Fonseca, M.P. Morales, J. Appl. Phys. 94 (2003) 3520.
[44] P. Dutta, S. Pal, M.S. Seehra, N. Shah, G.P. Huffman, J. Appl. Phys. 105 (2009) 07B501.
[45] S. Ayyappan, G. Panneerselvam, M.P. Antony, N.V. Rama Rao, N. Thirumurugan, A. Bharathi, J. Philip, J. Appl. Phys. 109 (2011) 084303.
[46] S. Larumbe, C. Gómez-Polo, J.I. Pérez-Landazábal, J.M. Pastor, J. Phys. Condens. Matter 24 (2012) 266007.